# Temperature-Insensitive Piezoelectric Performance in Pb(Zr$_{0.52}$Ti$_{0.42}$Sn$_{0.02}$Nb$_{0.04}$)O$_3$ Ceramics Prepared by Spark Plasma Sintering

Bing Han,[†,‖] Chunlin Zhao,[‡,‖] Zhi-Xiang Zhu,*[,§] Xin Chen,[§] Yu Han,[§] Duan Hu,[‡] Mao-Hua Zhang,[‡] Hao Cheng Thong,[‡] and Ke Wang*[,‡]

[†]Department of Orthodontics, Peking University School and Hospital of Stomatology, National Engineering Laboratory for Digital and Material Technology of Stomatology, Beijing Key Laboratory of Digital Stomatology, Beijing 100081, P. R. China

[‡]State Key Laboratory of New Ceramics and Fine Processing, School of Materials Science and Engineering, Tsinghua University, Beijing 100084, P. R. China

[§]Department of New Electrical Materials, State Grid Smart Grid Research Institute, Changping District, Beijing 102209, P. R. China

**ABSTRACT:** Dense Pb(Zr$_{0.52}$Ti$_{0.42}$Sn$_{0.02}$Nb$_{0.04}$)O$_3$ high-performance piezoceramics were prepared by spark plasma sintering. Phase structure, domain structure, and temperature-dependent electrical properties were systematically investigated. The spark-plasma-sintered ceramics possess a pure perovskite structure with rhombohedral−tetragonal (R−T) phase boundaries and a high Curie temperature of 347 °C. Reliable performance against temperature was observed. First, high strain behavior with a normalized strain $d_{33}^*$ of 640 and 710 pm/V occurred at 25 and 150 °C, respectively, varying less than 11%. Besides, a large remnant polarization $P_r$ of 36.9 $\mu$C/cm$^2$ is observed at room temperature and varies less than 18% within the temperature range of 25−150 °C. In addition, an enhanced piezoelectric coefficient $d_{33}$ of ∼460 pm/V was attained at a high temperature of 150 °C, manifesting a 40% enhancement with respect to the $d_{33}$ value (330 pm/V) obtained at room temperature.

**KEYWORDS:** piezoceramics, lead-based, spark plasma sintering, electrical properties, temperature reliability
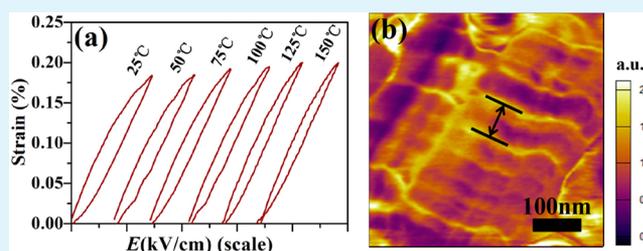
## 1. INTRODUCTION

Over the past decades, a great demand for robust electromechanical devices with the function of interconverting electrical energy and mechanical energy has grown dramatically, especially in aerospace and automotive industries. As a core component of the electromechanical devices, piezoelectric materials are frequently subjected to rigorous conditions, for example, high power load and high service temperature, which are of the utmost importance. Hence, materials with both good piezoelectricity and thermal stability are preferred.[1−15] Piezoelectric actuator is one of the significant interests in electromechanical applications, which was expected to possess a global market of $12 290 million in 2014.[1] Performance of the piezoelectric actuator can be evaluated by different figures of merit, such as normalized strain $d_{33}^*$ and Curie temperature $T_C$. Optimizations on these figures of merit are necessary for designs of commercial product.[1,2] Until now, lead-based perovskite piezoelectric materials have still firmly dominated the commercial electronic devices market, such as sensors, bimorphs, actuators, transducers, and ultrasonic motors, due to their excellent piezoelectric properties and high reliability.[2,3] An enhanced performance of lead-based piezoelectric ceramics can be obtained when the composition/temperature is close to the morphotropic phase boundaries (abbreviated as MPB).[3,4]

It is worth noting that lead-based ceramics can be categorized into two major groups according to the need of applications. The first group refers to the applications that require reliable room-temperature piezoelectric performance, without much concern with temperature stability, such as transducers and infrared detectors.[5] By contrast, temperature insensitivity receives more attention for the second group, such as sensors.[6] To further improve the robustness, regardless of the different application scopes, effort should be paid to the study of temperature dependence of electric performance for lead-based and lead-free piezoelectric ceramics.[7−15,34−38] In addition, the performance of piezoelectric ceramics strongly depends on the methods of fabrication, which includes normal sintering,[16−18] hot-pressing sintering,[19] spark plasma sintering (SPS),[20,21] and so on. For the normal sintering of lead-based ceramics, a high sintering temperature (1200−1300 °C) is usually required to obtain an eligible perovskite structure for the sake of high performance. However, appearance of a liquid phase during high-temperature sintering can easily cause abnormal grain growth, which can deteriorate the piezoelectric properties.
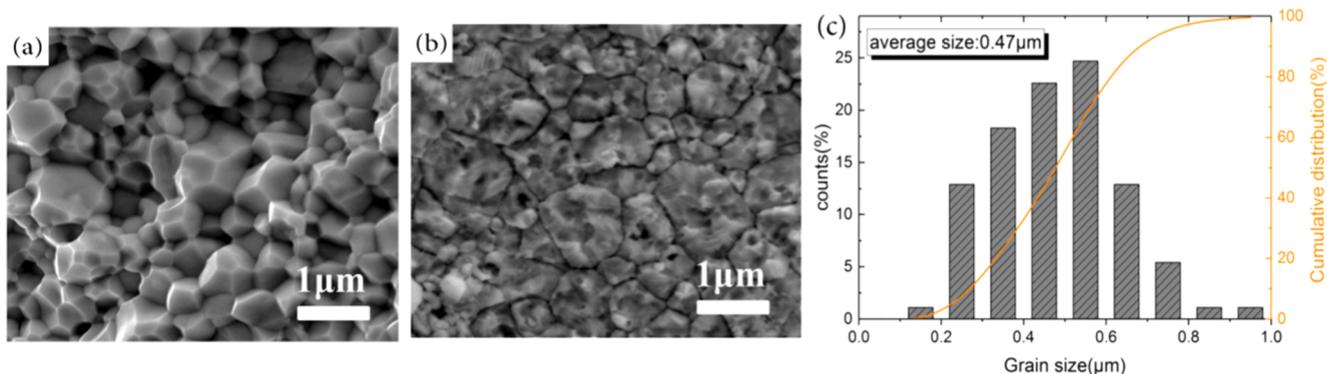
**Figure 1.** Field emission scanning electron microscopy images of spark-plasma-sintered PSN ceramics with (a) cross section, (b) surface after chemical etching, and (c) grain size distribution.

**Table 1. Electrical Properties of Spark-Plasma-Sintered PSN Ceramics Sintered at 1050 °C for 5 min**

| $T_m$ (°C) | Strain (%)/3 kV/mm | $d_{33}$* (pm/V) | $d_{33}$ (pC/N) | $P_r$ ($\mu$C/cm$^2$) | $E_c$ (kV/mm) | $\varepsilon_r$ (1 kHz) | tan $\delta$ (1 kHz) | $T_C$ (°C) | $\rho$ (g/cm$^3$) |
|---|---|---|---|---|---|---|---|---|---|
| 25 | 0.187 | 640 | 350 | 36.9 | 1.7 | 1350 | 0.021 | 347 | 7.64 |
| 150 | 0.241 | 710 | 465 | 31.0 | 1.1 | 2295 | 0.017 | | |

Thus, obtaining a highly dense structure without an abnormal grain growth is preferred in lead-based systems. Surprisingly, spark plasma sintering (SPS) is well known for reducing the sintering temperatures by about 200−300 °C while maintaining a high relative density (>99%), providing a promising alternative to fabricate the lead-based ceramics with high mechanical strength and homogeneous fine-grain sizes.[20−23] However, there are few comprehensive reports on the temperature dependence of electrical properties (e.g., ferroelectric, piezoelectric, dielectric, strain properties) for SPS-synthesized lead-based ceramics. It is therefore worth investigating the temperature-dependent properties of lead-based ceramics prepared by the SPS method.

Among all of the lead-based piezoelectric ceramics, PZT ceramics with additions of Sn and Nb possess a unique nanoscale structure, which is able to optimize the electrical properties.[24−26] In this work, Sn and Nb co-doped PZT ceramics with nominal chemical composition Pb-($Zr_{0.52}Ti_{0.42}Sn_{0.02}Nb_{0.04}$)O$_3$ were prepared by the SPS method. Temperature dependence of the electrical properties was systematically investigated. The spark-plasma-sintered ceramics were found to possess high piezoelectric and dielectric properties at a high-temperature region, as well as good strain and ferroelectric performance with an excellent temperature stability from 25 to 150 °C. This work demonstrates that SPS is an effective method for obtaining high-performance lead-based piezoceramics, which is believed to be beneficial for further applications of both lead-based and lead-free piezoelectric ceramics.

## 2. EXPERIMENTAL SECTION

Commercial Pb$_3$O$_4$ (95.0%), ZrO$_2$ (99.0%), TiO$_2$ (98.0%), SnO$_2$ (99.5%), and Nb$_2$O$_5$ (99.5%) were mixed according to the nominal composition Pb($Zr_{0.52}Ti_{0.42}Sn_{0.02}Nb_{0.04}$)O$_3$ (PSN). The raw materials were weighed stoichiometrically and then ball milled for 24 h in the ethanol solution. The mixed powders were calcined at 850 °C for 2 h. The SPS apparatus (Dr. Sinter 1020 SPS, Sumitomo Coal Mining Co. Ltd., Kawasaki, Japan) was used to prepare the PSN ceramic samples. Approximately 5 g of calcined PSN powder was compacted into a SPS graphite die with an inner diameter of 10 mm. As spark-plasma-sintered ceramics generally require a sintering temperature 100−200 °C lower than the conventional solid-state method, an SPS

temperature of 1050 °C was used to sinter the PSN ceramics. After the SPS chamber was evacuated (6−8 Pa), the samples were heated to the selected temperature at a rate of 100 °C/min and held for 5 min. A constant pressure of 50 MPa was applied to the powder inside the graphite die along the Z axis before the temperature reached 1050 °C. The applied voltage was adjusted accordingly to the heating rate and the selected sintering temperature. The graphite die was cooled naturally to 200 °C, after which the sintered samples were taken out and cut into disks with a thickness of 1 mm. Postannealing was then carried out in two steps. First, the SPS samples were annealed in air at 700 °C for 4 h, followed by annealing in air at 1000 °C for 6 h to eliminate oxygen vacancies formed during the SPS process. Finally, the sintered disks were coated with silver paste on the upper and bottom surfaces and then kept at 600 °C for 10 min to form electrodes for electrical measurements.

The average density $\rho$ of the as-sintered ceramic was determined by the Archimedes method using several pellets. Phase structures of the sintered disks were analyzed by X-ray diffraction (XRD) with a Cu K$\alpha$ radiation (Rigaku, D/Max250, Tokyo, Japan). Surface morphology was observed by a field emission scanning electron microscope (JEOL, JSM-6SOFF, Japan). Piezoresponse force microscopy experiments were carried out using a commercial atomic force microscope MFP-3D (Asylum Research). Temperature-dependent dielectric constant and dielectric loss were determined with an impedance analyzer (TH2827, Changzhou Tonghui Electronic Co, China). Temperature-dependent ferroelectric properties, unipolar piezoelectric strain $S(E)$ curves, and field-dependent piezoelectric coefficient $d_{33}(E)$ hysteresis loops were measured with a ferroelectric tester (aixACCT TF Analyzer 1000, Germany). A bipolar electric field of 3 kV/mm at 1 Hz was applied to obtain polarization $P(E)$ hysteresis loops. Unipolar strain hysteresis was obtained with a unipolar triangular signal of 3 kV/mm at 1 Hz. $d_{33}(E)$ hysteresis loops, permittivity $\varepsilon(E)$ curves, and dissipation factor tan $\delta$ ($E$) curves were measured by applying a triangular signal of 3 kV/mm at a frequency of 1 Hz, on which an AC voltage of 25 V at 250 Hz was superimposed.

## 3. RESULTS AND DISCUSSION

Figure 1a,b shows the cross-sectional and surface scanning electron microscopy (SEM) images of the spark-plasma-sintered PSN ceramics, respectively. Dense structure and fine grain with an average grain size of ∼0.47 $\mu$m were observed. Table 1 shows the electrical properties of the spark-plasma-sintered PSN ceramics sintered at a low temperature of 1050 °C for 5 min. Measurements were carried out at the

temperatures of 25 and 150 °C (denoted by $T_m$). It can be seen that the spark-plasma-sintered PSN ceramics have a relatively high density of 7.64 g/cm$^3$ and good electrical properties. At an elevated temperature of ~150 °C, the ceramics exhibit enhanced strain and piezoelectric properties, including both piezoelectric coefficient $d_{33}$ and normalized strain $d_{33}$*. Dielectric performance is also improved. However, ferroelectric properties, evaluated from the remnant polarization $P_r$, deteriorate when the temperature increases from 25 to 150 °C. More importantly, the ceramics attain a high $T_C$ of 347 °C, which is promising for practical applications, due to a wide operating temperature range.[2,5]

Figure 2a,b shows the room-temperature XRD patterns of the PSN lead-based ceramics synthesized by spark plasma
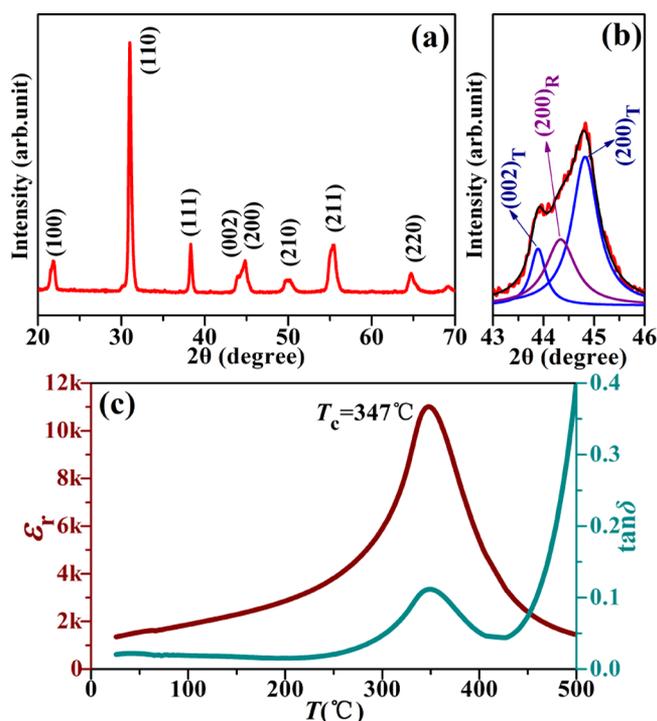


**Figure 2.** (a) XRD pattern of the as-sintered PSN ceramics. (b) Corresponding XRD patterns at $2\theta$ = 43−46°. (c) Temperature dependence of dielectric permittivity and dielectric loss of poled PSN ceramic measured at 1 kHz.

sintering, measured at a $2\theta$ range from 20 to 70° and room temperature of ~20 °C. To further judge its phase evolution, magnified XRD patterns at $2\theta$ = 43−46° are also displayed. As shown in Figure 2a, the sample possesses a pure perovskite structure, indicating that all of the elements, including Sn and Nb, diffuse into the ceramic lattice to form a solid solution. It is well accepted that the piezoelectricity of lead-based ceramics is greatly dependent on the phase structures, which can be characterized by the diffraction peak around $2\theta$ of 43−46°, as shown in the magnified XRD pattern in Figure 2b. The peak overlap is observed in the XRD pattern, where a merged peak is shown within this characteristic $2\theta$ range. Therefore, Lorentz distribution is used for fitting the merged peak. Lorentz fitting result shows that the merged peak consists of three single peaks. The left and right sides of the merged peak represent (002) and (200) of the tetragonal (T) phase, and the middle peak represents (200) of the rhombohedral (R) phase.[7] Therefore, the coexistence of both T and R phases shown in

the XRD pattern suggests that an R−T phase boundary appears in this system. The XRD results can be supported by the temperature-dependent dielectric permittivity ($\varepsilon_r$−$T$ curves) and the dielectric loss (tan $\delta$−$T$ curves) result measured by an impedance analyzer, as shown in Figure 2c. An anomalous peak is observed at 347 °C in the dielectric constant curve, which corresponds to the phase transition temperature from a tetragonal phase to a cubic phase ($T_C$). The coexistence of R phase and T phase can account for the enhanced electrical properties of the PSN ceramics,[3,4] as shown in Table 1 and subsequent discussions. The coexistence of R and T phases is further proved by the nanosized domain structure, as shown in Figure 3, which is in accordance with previous studies.[27,28] Also, the nanodomain structure should be partly responsible for the enhanced piezoelectric properties.[29]

Figure 4 shows the temperature dependence of permittivity $\varepsilon(E)$ curves and dielectric loss factor tan $\delta$ curves of PSN ceramics measured from 25 to 150 °C by using a ferroelectric tester. It can be seen from Figure 4a that the $\varepsilon(E)$ curves move upward along the $Y$ axis (permittivity axis) with increasing temperature, indicating that the dielectric constant of the ceramics improves when the temperature is increased. Figure 4b displays the tan $\delta$ curves against the temperature. Two symmetrical loss peaks can be observed in both positive and negative electric fields. With increasing temperature, the tan $\delta$ curve always maintains its symmetry. Additionally, the loss peak gradually shifts to a lower electric field with increasing temperature. To identify the normal dielectric properties against temperature the intercept values of permittivity and dielectric loss factor curves on $Y$-axis are plotted in Figure 4c,d. In Figure 4c, the permittivity is found to increase linearly with temperature. The room-temperature permittivity is about 1600, whereas the permittivity at 150 °C is about 2700. Nevertheless, the dielectric loss factor remains almost unchanged, as shown in Figure 4d. The variation in the dielectric loss factor is less than 7.5% within the wide temperature range, indicating a good temperature stability. Furthermore, the permittivity and the dielectric loss results measured by the impedance analyzer, which is been shown in Figure 2c, are also shown with dash lines in Figure 4c,d, respectively. The results obtained from the two different measurement techniques are in good agreement, yet the difference in the concrete values between the two curves should be attributed to the different test frequencies, which are 1 kHz and 250 Hz for the impedance analyzer and the ferroelectric tester, respectively.[30]

Figure 5a,e displays the polarization hysteresis $P(E)$ loops and the field-dependent piezoelectric coefficient $d_{33}(E)$ hysteresis loops measured at different temperatures, respectively. Saturated $P(E)$ loops are observed in Figure 5a for all of the measured temperatures. As the temperature increases, it can be seen that the ferroelectric loops gradually become slim, and the $P_s$, $P_r$, and $E_c$ values of the $P(E)$ loops all decline with an increase in the temperature, as shown in Figure 5b−d. When the samples are heated to 150 °C from the room temperature, $P_s$ decreases from 42.3 to 39.3 $\mu$C/cm$^2$ and $P_r$ decreases from 36.9 to 31.0 $\mu$C/cm$^2$. Considering the limited reduction in remnant polarization, the ferroelectric properties of SPS-synthesized PSN ceramics are considered to be temperature-insensitive. In addition, decrease in $E_c$ with an increase in temperature indicates that it is easier for the domain-wall motion at a higher temperature. Figure 5e displays the field-dependent $d_{33}(E)$ hysteresis loops. The intercept in $X$ axis of loops gradually decreases with increase in temperature, whereas
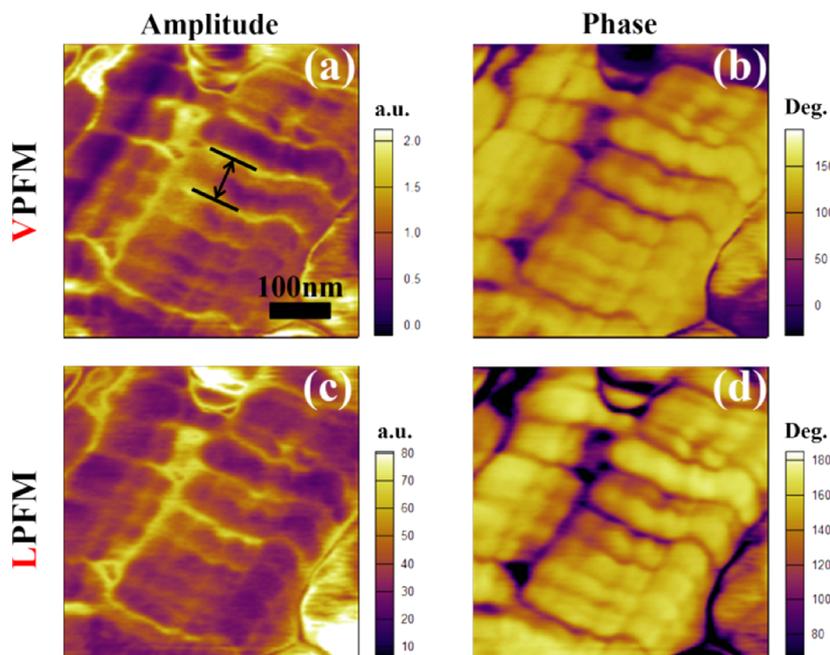
**Figure 3.** Domain configurations of the ceramics through vector piezoresponse force microscopy. (a, b) Vertical and (c, d) lateral piezoresponse amplitude and phase images, where nanosized domain structure is easily observed.
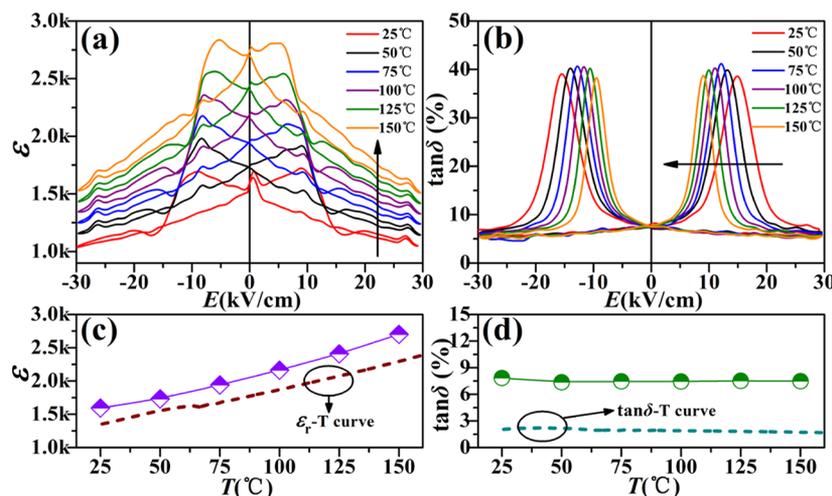


**Figure 4.** Temperature-dependent (a) permittivity $\varepsilon(E)$ curves and (b) dielectric loss factor $\tan \delta$ curves. (c) Positive $Y$-intercept of the electric-field-induced permittivity and the (d) positive $Y$-intercept values of the dielectric loss factor at different measurement temperature. The dotted lines are the results of temperature dependence of dielectric constant and dielectric loss curves measured by the impedance analyzer.

the intercept in $Y$ axis increases. The positive intercept in the $Y$ axis of a $d_{33}(E)$ loop can be defined as normal piezoelectric coefficient, $d_{33}$.[12] Hence, Figure 5e shows that $d_{33}$ is about 330 pm/V at room temperature and increases to 460 pm/V at 150 °C, exhibiting a 40% enhancement compared with the value obtained at room temperature. Instead of deteriorating, with increasing temperature, a better piezoelectric performance is observed, as seen in Figure 5f. This result agrees with the phenomenon that lead-based ceramics usually obtain a superior piezoelectric performance when poled at a high temperature. It is widely believed that the intrinsic contribution of MPB and a high Curie temperature account for the enhancement. At a high temperature (but still far below $T_C$), the process of polarization, or domain rotation and extension, may become easier due to thermal activity.[12,31,34−36] A similar phenomenon was also

observed in the strain performance of the SPS-synthesized PSN ceramics, as will be subsequently discussed.

Figure 6a shows the bipolar strain curves measured at different temperatures. It can be seen that the $S(E)$ curves gradually become slim, and both the poling strain $S_{pol}$ and the negative strain $S_{neg}$ decrease when the temperature increases, whereas the positive strain $S_{pos}$ enhances slightly, as shown in Figure 6b−d. As the temperature rises from 25 to 150 °C, the $S_{pos}$ values increase from 0.187 to 0.241%. In contrast, $S_{neg}$ values decrease from 0.207 to 0.108%. It has been previously reported that the magnitude of $S_{neg}$ depends on the competition between non-180° and 180° domain-switching processes. A higher $S_{neg}$ value indicates a larger proportion of non-180° domain switching.[31,32] Hence, the observed decrease in $S_{neg}$ should be due to less non-180° domain-switching processes occurring at the elevated temperature.[33] The
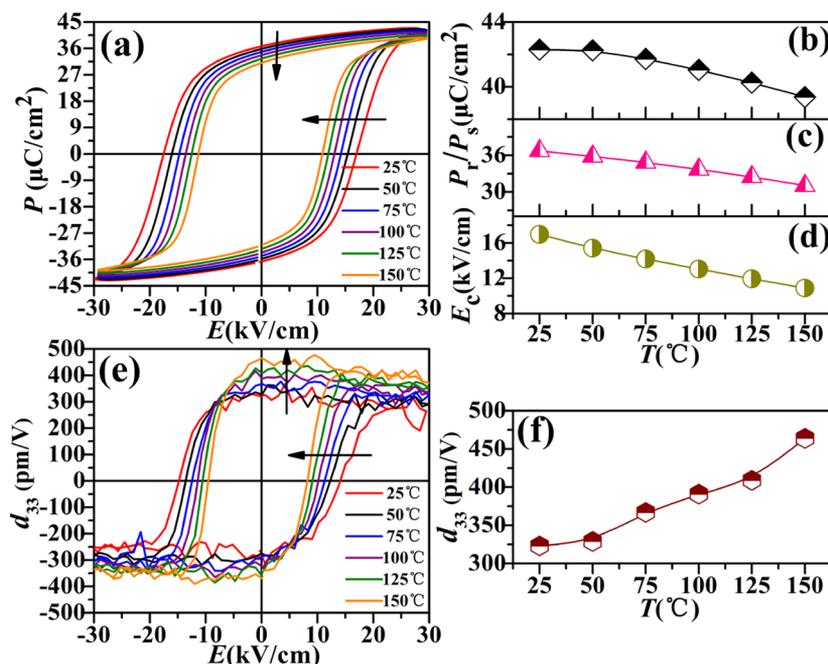
**Figure 5.** Temperature-dependent (a) ferroelectric loops $P(E)$, (b−d) $P_s$, $P_r$, and $E_c$, (e) piezoelectric coefficient $d_{33}(E)$ hysteresis loops, and (f) the positive $Y$-intercept values of each $d_{33}(E)$ loops.
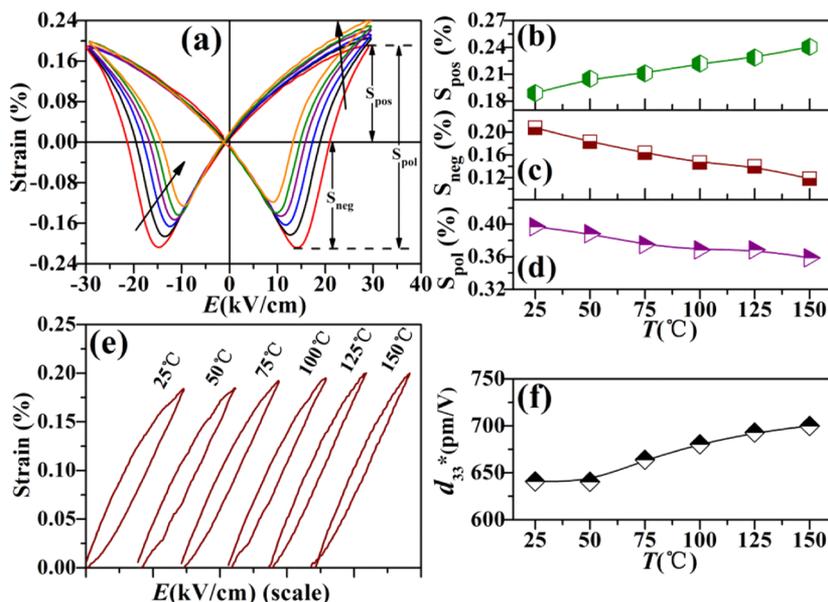


**Figure 6.** Temperature-dependent (a) bipolar strain curves $S(E)$, (e) unipolar piezoelectric strain curves, (b−d) $S_{pos}$, $S_{neg}$, and $S_{pol}$, and (f) the inverse piezoelectric coefficient $d_{33}*$.

enhanced $S_{pos}$ with rising temperature can be partly attributed to the suppression of the negative strain, as in some high-strain systems of the piezoelectric ceramics.[32] Additionally, we can see from Figure 6a that the $S(E)$ curves present asymmetric characteristics along the $Y$ axis. The asymmetry could possibly be the result of an internal bias field created by the repeatedly applied electric field during measurements. Moreover, high temperature actually facilitates the accumulation of space charge carriers that are responsible for the formation of this bias field.[39,40] Figure 6e displays the unipolar piezoelectric strain curves measured at different temperatures and an electric field of 3 kV/mm. Most of the time, the unipolar strain is a useful figure of merit, especially for actuating devices. The strain

of ∼0.19% for the PSN ceramics at 25 °C gradually increases to ∼0.21% at 150 °C. The normalized strain $d_{33}*$ (calculated by $S_{max}/E_{max}$ according to the unipolar strain curves) correspondingly improves from 640 to 710 pm/V (see Figure 6c). Moreover, the ascended unipolar strain is consistent with the enhanced $S_{pos}$ of the bipolar strain. As discussed above, it is assumed that this result should originate from the thermal activity and a more severe degradation of $P_r$ than of $P_s$ with the increasing temperature,[9] as shown in Figure 5b,c. Due to the unipolar strain, $S_{uni}$ is related to the remanent polarization $P_r$ and the maximum polarization $P_s$ as written in eq 1

$$S_{uni} = S_{max} - S_{rem} = Q\,P_s^2 - Q\,P_r^2 = Q(P_s^2 - P_r^2) \qquad (1)$$

where $Q$ is the electrostrictive constant. As shown in Figure 7a, $P_s^2 - P_r^2$ gradually increases with increase in the temperature, yielding an enhanced unipolar strain.[9]
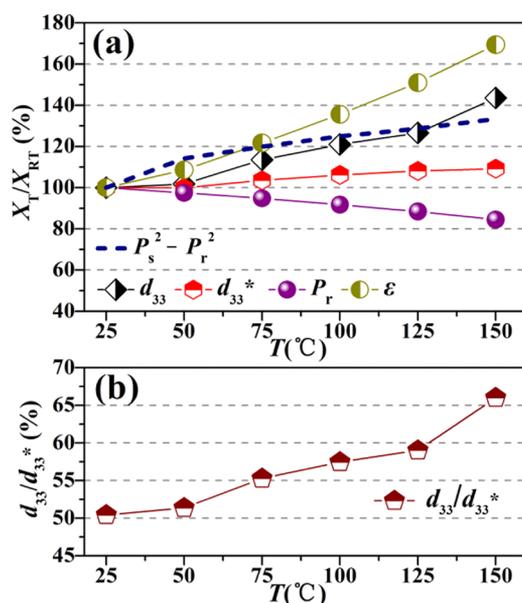


**Figure 7.** (a) Normalized $X$ ($X = d_{33}*$, $d_{33}$, $P_r$, $\varepsilon$, and $P_s^2 - P_r^2$) parameters against their room temperature values. (b) Temperature-dependent $d_{33}/d_{33}*$ from 25 to 150 °C.

As shown in Figure 7a, except for ferroelectric polarization, almost all of the measured electric properties of the spark-plasma-sintered PSN lead-based piezoelectric ceramic exhibit a rising trend in the temperature range of 25−150 °C. The 40% enhancement in the piezoelectric coefficient $d_{33}$ and the 70% improvement in the dielectric constant $\varepsilon$ obtained at 150 °C suggest a better prospect in high-temperature application for this ceramics. On the other hand, an excellent temperature stability with a variation of less than 11% for the normalized strain $d_{33}*$ is exhibited in a wide temperature range of 25−150 °C, indicating that the spark-plasma-sintered PSN ceramics are highly suited for the devices requiring a broad temperature stability of properties. The high remnant polarization $P_r$, fluctuating less than 18% within the range of 25−150 °C, is favorable for ferroelectric devices. In addition, the ratio of $d_{33}/d_{33}*$ at different temperatures is illustrated in Figure 7b. One can see that the piezoelectric coefficient $d_{33}$ is always smaller than the normalized strain $d_{33}*$; however, the ratio gradually increases from 0.50 to 0.65 with increasing temperature. This phenomenon may originate from the constitution of the piezoelectric effect. It is well known that both intrinsic and extrinsic piezoelectric responses contribute to the piezo-electricity. The intrinsic contribution of the lattice structure should be temperature-insensitive, whereas the extrinsic component of the domain rotation and extension is sensitive to the external temperature fluctuation. As aforementioned, the domain rotation and extension will be facilitated at a higher temperature due to the reduced barriers for domain switching, resulting in an enhanced ratio between $d_{33}$ and $d_{33}*$.

## 4. CONCLUSIONS

The structural and temperature-dependent characteristics of the electrical properties of dense PSN piezoelectric ceramics synthesized using the spark plasma sintering method were systematically analyzed. The temperature dependence of dielectric, ferroelectric, piezoelectric, and strain properties were investigated. The dielectric and piezoelectric constant possess superior values at higher temperature, whereas the ferroelectric properties and the field-induced strain show a significant temperature insensitivity. In the near future, these characteristics might lead to various practical applications that require temperature stability.

## ■ AUTHOR INFORMATION

**Corresponding Authors**
*E-mail: zhuzhixiang003@163.com (Z.-X.Z.).
*E-mail: wang-ke@tsinghua.edu.cn (K.W.).

**ORCID** ⬢
Ke Wang: 0000-0001-9840-2427

**Author Contributions**
∥B.H. and C.Z. contributed equally to this work.

**Notes**
The authors declare no competing financial interest.

## ■ REFERENCES

(1) Jo, W.; Dittmer, R.; Acosta, M.; Zang, J.; Groh, C.; Sapper, E.; Wang, K.; Rödel, J. Giant Electric-Field-Induced Strains in Lead-Free Ceramics for Actuator Applications-Status and Perspective. *J. Electroceram.* **2012**, *29*, 71−93.

(2) Setter, N. *Piezoelectric Materials and Devices*; Ceramics Laboratory, EPFL Swiss Federal Institute of Technology: Lausanne, 2005.

(3) Jaffe, B.; Cook, W. R.; Jaffe, H. *Piezoelectric Ceramics*; Academic Press Ltd.: London, 1971.

(4) Fu, H.; Cohen, R. E. Polarization Rotation Mechanism for Ultrahigh Electromechanical Response in Single-Crystal Piezoelectrics. *Nature* **2000**, *403*, 281−283.

(5) Zhang, S. J.; Xia, R.; Lebrun, L.; Anderson, D.; Shrout, T. R. Piezoelectric Materials for High Power, High Temperature Applications. *Mater. Lett.* **2005**, *59*, 3471−3475.

(6) Turner, R. C.; Fuierer, P. A.; Newnham, R. E.; Shrout, T. R. 'Materials for High Temperature Acoustic and Vibration Sensors: A Review. *Appl. Acoust.* **1994**, *41*, 299−324.

(7) Luo, N. N.; Li, Q.; Xia, Z. G.; Chu, X. C. Phase Diagram, Temperature Stability, and Electrical Properties of (0.85-$x$)Pb-$(Mg_{1/3}Nb_{2/3})O_3$−0.10Pb $(Fe_{1/2}Nb_{1/2})O_3$−0.05PbZrO₃−$x$PbTiO₃ System. *J. Am. Ceram. Soc.* **2012**, *95*, 3246−3253.

(8) Wang, D. W.; Cao, M. S.; Zhang, S. J. Piezoelectric Ceramics in the PbSnO₃-Pb$(Mg_{1/3}Nb_{2/3})O_3$-PbTiO₃ Ternary System. *J. Am. Ceram. Soc.* **2011**, *94*, 3690−3693.

(9) Wang, K.; Yao, F.-Z.; Jo, W.; Gobeljic, D.; Shvartsman, V. V.; Lupascu, D. C.; Li, J.-F.; Rödel, J. Temperature-Insensitive (K,Na)-NbO₃-Based Lead-Free Piezoactuator Ceramics. *Adv. Funct. Mater.* **2013**, *23*, 4079−4086.

(10) Yao, F. Z.; Wang, K.; Jo, W.; Webber, K. G.; Comyn, T. P.; Ding, J.-X.; Xu, B.; Cheng, L.-Q.; Zheng, M.-P.; Hou, Y.-D.; Li, J.-F. Diffused Phase Transition Boosts Thermal Stability of High-Performance Lead-Free Piezoelectrics. *Adv. Funct. Mater.* **2016**, *26*, 1217−1224.

(11) Wu, J. G.; Xiao, D. Q.; Zhu, J. G. Potassium-Sodium Niobate Lead-Free Piezoelectric Materials: Past, Present, and Future of Phase Boundaries. *Chem. Rev.* **2015**, *115*, 2559−2595.

(12) Yao, F.-Z.; Yu, Q.; Wang, K.; Li, Q.; Li, J.-F. Ferroelectric Domain Morphology and Temperature-Dependent Piezoelectricity of $(K,Na,Li)(Nb,Ta, Sb)O_3$ Lead-Free Piezoceramics. *RSC Adv.* **2014**, *4*, 20062−20068.

(13) Zheng, T.; Wu, H. J.; Yuan, Y.; Lv, X.; Li, Q.; Men, T. L.; Zhao, C. L.; Xiao, D. Q.; Wu, J. G.; Wang, K.; Li, J.-F.; Gu, Y. L.; Zhu, J. G.; Pennycook, S. J. The Structural Origin of Enhanced Piezoelectric Performance and Stability in Lead Free Ceramics. *Energy Environ. Sci.* **2017**, *10*, 528−537.

(14) Zhang, M.-H.; Wang, K.; Du, Y.-J.; Dai, G.; Sun, W.; Li, G.; Hu, D.; Thong, H. C.; Zhao, C. L.; Xi, X.-Q.; Yue, Z.-X.; Li, J.-F. High and Temperature-Insensitive Piezoelectric Strain in Alkali Niobate Lead-free Perovskite. *J. Am. Chem. Soc.* **2017**, *139*, 3889−3895.

(15) Wu, J. G.; Fan, Z.; Xiao, D. Q.; Zhu, J. G.; Wang, J. Multiferroic bismuth ferrite-based materials for multifunctional applications: Ceramic bulks, thin films and nanostructures. *Prog. Mater. Sci.* **2016**, *84*, 335−402.

(16) Wittmer, D. E.; Buchanan, R. C. Low-Temperature Densification of Lead Zirconate-Titanate with Vanadium Pentoxide Additive. *J. Am. Ceram. Soc.* **1981**, *64*, 485−490.

(17) Wu, J. G.; Xiao, D. Q.; Wang, Y. Y.; Wu, L.; Jiang, Y. H.; Zhu, J. G. K/Na Ratio Dependence of the Electrical Properties of $[(K_xNa_{1-x})_{0.95}Li_{0.05}](Nb_{0.95}Ta_{0.05})O_3$ Lead-Free Ceramics. *J. Am. Ceram. Soc.* **2008**, *91*, 2385−2387.

(18) Wang, K.; Li, J.-F.; Liu, N. Piezoelectric Properties of Low-Temperature Sintered Li-Modified $(Na,K)NbO_3$ Lead-Free Ceramics. *Appl. Phys. Lett.* **2008**, *93*, No. 092904.

(19) Kingon, A. I.; Clark, J. B. Sintering of PZT Ceramics: II, Effect of PbO Content on Densification Kinetics. *J. Am. Ceram. Soc.* **1983**, *66*, 256−260.

(20) Zhang, B.-P.; Li, J.-F.; Wang, K.; Zhang, H. Compositional Dependence of Piezoelectric Properties in NaxK1xNbO3 Lead-Free Ceramics Prepared by Spark Plasma Sintering. *J. Am. Ceram. Soc.* **2006**, *89*, 1605−1609.

(21) Shen, Z. Y.; Li, J. F.; Wang, K.; Xu, S. Y.; Jiang, W.; Deng, Q. H. Electrical and Mechanical Properties of Fine-Grained Li/Ta-Modified $(Na, K)NbO_3$ Based Piezoceramics Prepared by Spark Plasma Sintering. *J. Am. Ceram. Soc.* **2010**, *93*, 1378−1383.

(22) Wang, K.; Li, J.-F.; Liu, N. Piezoelectric Properties of Low-Temperature Sintered Li-Modified $(Na,K)NbO_3$ Lead-Free Ceramics. *Appl. Phys. Lett.* **2008**, *93*, No. 092904.

(23) Li, J.-F.; Wang, K.; Zhu, F.-Y.; Cheng, L.-Q.; Yao, F.-Z. $(K,Na)NbO_3$-Based Lead-Free Piezoceramics: Fundamental Aspects, Processing Technologies, and Remaining Challenges. *J. Am. Ceram. Soc.* **2013**, *96*, 3677−3696.

(24) He, H.; Tan, X. Electric Field-Induced Transformation of Incommensurate Modulations in Antiferroelectric $Pb_{0.99}Nb_{0.02}[(Zr_{1-x}Sn_x)_{1-y}Ti_y]_{0.98}O_3$. *Phys. Rev. B* **2005**, *72*, No. 024102.

(25) Yoon, K. H.; Shin, H. C.; Park, J.; Kang, D. H. Effect of Textured $Pb(Zr_{1-x}Ti_x)O_3$ Seed Layer on Fatigue Properties of Ferroelectric $Pb_{0.99}[(Zr_{0.6}Sn_{0.4})_{0.85}Ti_{0.15}]_{0.98}Nb_{0.02}O_3$ Thin Films. *J. Appl. Phys.* **2002**, *92*, 2108−2111.

(26) Yu, Y.; Wu, J. G.; Zhao, T. L.; Dong, S. X.; Gu, H. S.; Hu, Y. M. $MnO_2$ Doped PSN−PZN−PZT Piezoelectric Ceramics for Resonant Actuator Application. *J. Alloys Compd.* **2014**, *615*, 676−682.

(27) Asada, T.; Koyama, Y. Ferroelectric Domain Structures Around the Morphotropic Phase Boundary of the Piezoelectric Material $PbZr_{1-x}Ti_xO_3$. *Phys. Rev. B* **2007**, *75*, No. 214111.

(28) Lummen, T. T.; Gu, Y.; Wang, J.; Lei, S.; Xue, F.; Kumar, A.; Barnes, A. T.; Barnes, E.; Denev, S.; Belianinov, A.; Holt, M.; Morozovska, A. N.; Kalinin, S. V.; Chen, L.-Q.; Gopalan, V. Thermotropic Phase Boundaries in Classic Ferroelectrics. *Nat. Commun.* **2014**, *5*, No. 3172.

(29) Xu, K.; Li, J.; Lv, X.; Wu, J. G.; Zhang, X. X.; Xiao, D. Q.; Zhu, J. G. Superior Piezoelectric Properties in Potassium Sodium Niobate Lead-Free Ceramics. *Adv. Mater.* **2016**, *28*, 8519−8523.

(30) Leist, T.; Chen, J.; Jo, W.; Aulbach, E.; Suffner, J.; Rödel, J. Temperature Dependence of the Piezoelectric Coefficient in $BiMeO_3$-$PbTiO_3$ (Me = Fe, Sc, $(Mg_{1/2}Ti_{1/2})$) Ceramics. *J. Am. Ceram. Soc.* **2012**, *95*, 711−715.

(31) Chen, J.; Tan, X.; Jo, W.; Rödel, J. Temperature Dependence of Piezoelectric Properties of High-$T_C$ $Bi(Mg_{1/2}Ti_{1/2})O_3$−$PbTiO_3$. *J. Appl. Phys.* **2009**, *106*, No. 034109.

(32) Jo, W.; Dittmer, R.; Acosta, M.; Zang, J.; Groh, C.; Sapper, E.; Wang, K.; Rödel, J. Giant Electric-Field-Induced Strains in Lead-Free Ceramics for Actuator Applications-Status and Perspective. *J. Electroceram.* **2012**, *29*, 71−93.

(33) Jo, W.; Granzow, T.; Aulbach, E.; Rödel, J.; Damjanovic, D. Origin of The Large Strain Response in $(K_{0.5}Na_{0.5})NbO_3$-Modified $(Bi_{0.5}Na_{0.5})TiO_3$−$BaTiO_3$ Lead-Free Piezoceramics. *J. Appl. Phys.* **2009**, *105*, No. 094102.

(34) Khesro, A.; Wang, D. W.; Hussain, F.; Sinclair, D. C.; Feteira, A.; Reaney, I. M. Temperature Stable and Fatigue Resistant Lead-Free Ceramics for Actuators. *Appl. Phys. Lett.* **2016**, *109*, No. 142907.

(35) Zheng, T.; Wu, W. J.; Wu, J. G.; Zhu, J. G.; Xiao, D. Q. Balanced Development of Piezoelectricity, Curie Temperature, and Temperature Stability in Potassium−Sodium Niobhrate Lead-Free Ceramics. *J. Mater. Chem. C* **2016**, *4*, 9779−9787.

(36) Kungl, H.; Hoffmann, M. J. Temperature Dependence of Poling Strain and Strain Under High Electric Fields in LaSr-Doped Morphotropic PZT and its Relation to Changes in Structural Characteristics. *Acta Mater.* **2007**, *55*, 5780−5791.

(37) Luo, N. N.; Li, Q.; Xia, Z. G.; Chu, X. C. Phase Diagram, Temperature Stability, and Electrical Properties of (0.85-$x$)Pb-$(Mg_{1/3}Nb_{2/3})O_3$-0.10Pb$(Fe_{1/2}Nb_{1/2})O_3$-0.05PbZrO$_3$−$x$PbTiO$_3$ System. *J. Am. Ceram. Soc.* **2012**, *95*, 3246−3253.

(38) Yan, Y. K.; Kumar, A.; Correa, M.; Cho, K.-H.; Katiyar, R. S.; Priya, S. Phase Transition and Temperature Stability of Piezoelectric Properties in Mn-Modified $Pb(Mg_{1/3}Nb_{2/3})O_3$-PbZrO$_3$-PbTiO$_3$ Ceramics. *Appl. Phys. Lett.* **2012**, *100*, No. 152902.

(39) Yao, F.-Z.; Glaum, J.; Wang, K.; Jo, W.; Rödel, J.; Li, J.-F. Fatigue-Free Unipolar Strain Behavior in $CaZrO_3$ and $MnO_2$ Co-Modified $(K,Na)NbO_3$-Based Lead Free Piezoceramics. *Appl. Phys. Lett.* **2013**, *103*, No. 192907.

(40) Balke, N.; Lupascu, D. C.; Granzow, T.; Rödel, J. Fatigue of Lead Zirconate Titanate Ceramics. I: Unipolar and DC Loading. *J. Am. Ceram. Soc.* **2007**, *90*, 1081−1087.